THE UNIVERSITY of EDINBURGH

Edinburgh Research Explorer

Superconductivity in NdFe1-xCoxAsO (0.05 NdCoAsO

Citation for published version:
Marcinkova, A, Grist, DAM, Margiolaki, I, Hansen, TC, Margadonna, S & Bos, J-WG 2010, 'Superconductivity in NdFe1-xCoxAsO (0.05 NdCoAsO', *Physical review B*, vol. 81, no. 6, 064511, pp. -. https://doi.org/10.1103/PhysRevB.81.064511

Digital Object Identifier (DOI):
10.1103/PhysRevB.81.064511

Link:
Link to publication record in Edinburgh Research Explorer

Document Version:
Publisher's PDF, also known as Version of record

Published In:
Physical review B

Publisher Rights Statement:
Copyright 2010 The American Physical Society.This article may be downloaded for personal use only. Any other use requires prior permission of the author and the American Physical Society.

General rights
Copyright for the publications made accessible via the Edinburgh Research Explorer is retained by the author(s) and / or other copyright owners and it is a condition of accessing these publications that users recognise and abide by the legal requirements associated with these rights.

Take down policy
The University of Edinburgh has made every reasonable effort to ensure that Edinburgh Research Explorer content complies with UK legislation. If you believe that the public display of this file breaches copyright please contact openaccess@ed.ac.uk providing details, and we will remove access to the work immediately and investigate your claim.

Download date: 07. May. 2023

Superconductivity in $NdFe_{1-x}Co_xAsO$ ($0.05 < x < 0.20$) and rare-earth magnetic ordering in NdCoAsO

Andrea Marcinkova,[1] David A. M. Grist,[1] Irene Margiolaki,[2] Thomas C. Hansen,[3] Serena Margadonna,[1] and Jan-Willem G. Bos[1,4]

[1]*School of Chemistry and Centre for Science at Extreme Conditions, University of Edinburgh, Edinburgh EH9 3JJ, United Kingdom*

[2]*European Synchrotron Radiation Facility, 39043 Grenoble, France*

[3]*Institute Laue Langevin, 38042 Grenoble, France*

[4]*Department of Chemistry–EPS, Heriot-Watt University, Edinburgh EH14 4AS, United Kingdom*

(Received 11 September 2009; revised manuscript received 22 December 2009; published 19 February 2010)

The phase diagram of $NdFe_{1-x}Co_xAsO$ for low cobalt substitution consists of a superconducting dome ($0.05 < x < 0.20$) with a maximum critical temperature of 16.5(2) K for $x=0.12$. The $x=1$ end member, NdCoAsO, is an itinerant ferromagnet ($T_C=85$ K) with an ordered moment of 0.30(1) μ_B at 15 K. Below $T_N=9$ K, Nd spin ordering results in the antiferromagnetic coupling of the existing ferromagnetic planes. Rietveld analysis reveals that the electronically important twofold tetrahedral angle increases from 111.4° to 115.7° in this series. Underdoped samples with $x=0.046(2)$ and $x=0.065(2)$ show distortions to the orthorhombic *Cmma* structure at 72(2) and 64(2) K, respectively. The temperature dependences of the critical fields $H_{c2}(T)$ near T_c are linear with almost identical slopes of 2.3(1) T K^{-1} for $x=0.065(2)$, $x=0.118(2)$, and $x=0.172(2)$. The estimated critical field $H_{c2}(0)$ and correlation length for optimally doped samples are 26(1) T and 36(1) Å. A comparison of the maximum reported critical temperatures of well-characterized cobalt-doped 122- and 1111-type superconductors is presented.

DOI: 10.1103/PhysRevB.81.064511 PACS number(s): 74.70.−b, 74.25.Dw

I. INTRODUCTION

The 2008 discovery[1] of high-T_c superconductivity based on iron arsenide layers has generated enormous interest (Refs. 2 and 3 and references therein). Presently, the most widely investigated systems are the 1111-type *R*FeAsO (*R* =La, rare-earth) and 122-type $AEFe_2As_2$ (*AE*=alkaline earth) superconductors. Both contain square planar Fe layers, with Fe tetrahedrally coordinated by As, which are kept apart by either *R*O layers or *AE* ions. The 1111-type superconductors were the first to be discovered and hold the current record for critical temperatures and fields (up to 55 K and of the order of 100 T), while single crystals of the 122's (T_c up to 38 K) are readily available making detailed physical property studies possible. Like the cuprates, the iron arsenides have an antiferromagnetic (AF) parent. In contrast to the cuprates, the parent materials are metallic and not Mott insulators. The magnetism is therefore not due to superexchange but to Fermi surface nesting in the two-dimensional band structure, which results in a spin-density wave (SDW) state.[4,5] The parent materials are rendered superconducting (SC) via chemical doping[2,3] or in some cases application of hydrostatic pressure.[6] Both electron- and hole-doped superconductors exist.[2,3] Most temperature-composition phase diagrams show a dome-shaped SC region and suggest the coexistence of magnetic order and superconductivity for underdoped samples.[7–11] An exception is the phase diagram of $LaFeAsO_{1-x}F_x$ where a discontinuous transition into the superconducting state is reported.[12] In the cuprate high-T_c superconductors, chemical substitutions on the copper site are detrimental to superconductivity. By contrast in the iron arsenides, direct substitution on the Fe site with a variety of transition metals is known to induce superconductivity. This was first reported for 1111-type $LaFe_{1-x}Co_xAsO$ with a maximum critical temperature of 13–14 K.[13] Other well-characterized cobalt-doped superconductors include 122-type $AE(Fe_{1-x}Co_x)_2As_2$ (*AE*=Ba, Sr, and Ca),[14–16] 1111-type $SmFe_{1-x}Co_xAsO$,[17] and 1111-type $CaFe_{1-x}Co_xAsF$.[18] The highest reported T_c for cobalt doping is 22 K and is found for $Ba(Fe_{1-x}Co_x)_2As_2$ and $CaFe_{1-x}Co_xAsF$. The twofold tetrahedral As-Fe-As angle (α) is an important electronic parameter with higher T_c's found as α tends to the ideal cubic value (109.5°).[8,19] Most forms of chemical doping result in a reduction in α and values closer to 109.5°. For example, indirect electron doping of NdFeAsO ($\alpha=111.4°$) via F substitution or O deficiency reduces α by ~0.4° and ~1° for optimally doped samples.[19,20] This is also true for hole-doped 122 systems such as $Ba_{1-x}K_xFe_2As_2$ where $\alpha=109.5°$ for samples with $T_c=38$ K ($x=0.4$) compared to $\alpha=111.2°$ for the parent material.[21] In contrast, our results show that α increases with cobalt substitution (~1° for $x=0.12$), which is expected to have an unfavorable effect and reduce T_c from what is possible for a given nominal doping level (x). This effect is common to all cobalt-doped superconductors but does not seem to have been explicitly pointed out in the literature.

The fully substituted $x=1$ samples are also of considerable interest. LaCoAsO is an itinerant ferromagnet[13,22] with an anomalous magnetization similar to MnSi and $Fe_xCo_{1-x}Si$.[23] $BaCo_2As_2$ is not ferromagnetic (FM) but is in close proximity to a FM quantum critical point.[24] The presence of Nd in the current $x=1$ composition offers the prospect of studying the interplay between rare-earth and transition-metal magnetism. In the case of the *R*FeAsO parent materials this has generated much interest and a variety of combined *R* and Fe magnetic structures have been reported.[25,26] In all cases, T_N of the *R* sublattice is much lower than T_{SDW} (~140 K) for the Fe magnetic order, and the weak *R*-Fe interaction is not considered crucial in explaining the higher T_c's observed for magnetic *R* ions.[20,25]

 ©2010 The American Physical Society

In this paper, the temperature-composition phase diagram for $NdFe_{1-x}Co_xAsO$ ($0 \leq x \leq 1$) is reported from a combination of synchrotron x-ray, neutron powder-diffraction, magnetic susceptibility, and electrical resistivity measurements. These measurements reveal a SC dome extending from $0.05 < x < 0.20$ with maximum $T_c = 16.5(2)$ K and $H_{c2}(0) = 26(1)$ T for $x = 0.12$. NdCoAsO is an itinerant ferromagnet ($T_C = 85$ K) that shows a transition to long-range AF order ($T_N = 9$ K) upon ordering of the rare-earth spins. This work follows on from our earlier investigations into the effects of electron (via F substitution)[20,27] and hole doping (via Ca and Sr substitution)[28,29] of the parent material NdFeAsO.

II. EXPERIMENTAL

Polycrystalline samples of the $NdFe_{1-x}Co_xAsO$ ($x_{nominal} = 0$, 0.05, 0.075, 0.10, 0.125, 0.15, 0.175, 0.20, 0.25, 0.50, and 1) were prepared using standard solid-state chemistry methods. Stoichiometric mixtures of NdAs, Fe_2O_3, Fe, Co_3O_4, and Co powders of at least 99.9% purity were mixed using mortar and pestle and pressed into pellets. The pellets were vacuum sealed into quartz tubes and heated for 48 h at 1150 °C for $0 \leq x_{nominal} \leq 0.25$ and at 1050 °C for $x_{nominal} = 0.5$ and $x_{nominal} = 1$. The reactions were initially done on a 0.5 g scale. Larger 2 g samples of $x_{nominal} = 0.075$, 0.125, 0.175, and 1 were prepared for neutron powder diffraction. The starting material NdAs was prepared by heating stoichiometric mixtures of Nd and As pieces at 850 °C for 2×12 h with an intermediate shaking of the sealed tube. Initial phase analysis was done using laboratory powder x-ray diffraction on a Bruker D8 AXS diffractometer with a Cu $K_{\alpha 1}$ radiation source. Zero field cooled (ZFC) and field cooled (FC) dc magnetic susceptibilities were measured using a Quantum Design Magnetic Property Measurement System (MPMS). The applied magnetic field (H) for the superconductivity tests was 20 Oe. The temperature dependence of the susceptibility of the $x_{nominal} = 1$ sample was measured in $H = 10$ kOe. The temperature and field dependences of the electrical resistivity were measured using the resistance option of a Quantum Design Physical Property Measurement System (PPMS). The resistivities were measured using the four point contact method on bars of approximately $1 \times 1 \times 5$ mm^3. Sintered samples tend to degrade into powder when not kept in a closed container. This does not affect the crystallinity or the diamagnetic response but prevented us from obtaining resistivity measurements for some of the reported samples. High-resolution synchrotron powder-diffraction measurements were done on the ID31 beamline at the European Synchrotron Radiation Facility in Grenoble. The x-ray wavelength used was 0.3994 Å and data were binned with a 0.02° step size between $0 \leq 2\theta \leq 35°$. The samples were contained in 0.5 mm diameter silica capillaries. Room-temperature patterns were collected for all prepared samples while selected samples ($x_{nominal} = 0.05, 0.075, 0.125, 1$) were studied as a function of temperature using shorter scans. Room-temperature neutron powder-diffraction patterns for $x_{nominal} = 0.075$, 0.125, 0.175, and 1 were collected on the D20 beamline[30] at the Institute Laue Langevin in Grenoble. The instrument was used in the high-flux setting with and $\lambda = 1.304$ Å (42° take-off angle, Cu monochromator). The samples were contained in 6 mm diameter vanadium cans and cooled in a standard orange cryostat. Variable temperature data were collected between 1.7 and 100 K for NdCoAsO at wavelength $\lambda = 2.419$ Å (42° take-off angle, pyrolytic graphite monochromator). Data were collected between $10 \leq 2\theta \leq 140°$ and binned with a 0.1° step size. Rietveld analysis of the collected powder-diffraction data was done using the GSAS suite of programs.[31] A pseudo-Voigt function using Stephens anisotropic peak broadening was used to describe the peak shape for the synchrotron x-ray diffraction data.[32]

III. STRUCTURE AND PROPERTIES OF NdCoAsO ($x = 1$)

The temperature dependence of the crystal structure of NdCoAsO was followed between room temperature (RT) and 5 K using synchrotron x-ray powder diffraction. No structural transitions were observed and the structure was described using the $P4/nmm$ structural model reported by Quebe *et al.*[33] The RT lattice constants, atomic parameters, selected bond lengths, and fit statistics are summarized in Table I. The refined lattice constants and fractional coordinates at 5 K are as follows: $a = 3.97940(1)$ Å, $c = 8.29849(3)$ Å, $z_{Nd} = 0.14264(4)$, and $z_{As} = 0.65071(7)$ [$\chi^2 = 4.1$, $wR_p = 9.5\%$, $R_p = 6.2\%$, and $R_F^2 = 2.4\%$]. The Co-As bond distance contracts moderately from 2.3546(3) Å at RT to 2.3501(3) Å at 5 K, while the tetrahedral angle remains almost constant with RT and 5 K values of 115.70(3)° and 115.69(4)°, respectively.

The dc magnetic susceptibility is shown in Fig. 1(a) and reveals a FM divergence of the susceptibility with $T_c = 85$ K followed by a transition to an AF state at $T_N = 9$ K. The Curie temperature was determined from the local maximum in $d\chi/dT$, while the Néel temperature was taken when $d\chi/dT$ changes sign [Fig. 1(a)]. Zero field cooled and field cooled curves collected in 1 T do not show any thermal hysteresis. The high-temperature susceptibility does not follow the Curie-Weiss law. To further investigate the magnetic properties, $M(H)$ isotherms were collected at 1.7, 50, and 100 K. These data are shown in the inset of Fig. 1(b). The main panel shows the derived Arrott plots, M^2 versus H/M, that were used to determine the nature of the magnetic ground state.[34] Extrapolation of the linear high-field behavior for a ferromagnet yields a negative H/M-axis intersect, while the same extrapolation for AF and paramagnetic (PM) states intersect the H/M axis at a positive value. At 1.7 and 100 K, the Arrott plots clearly indicate the absence of ferromagnetism and are consistent with antiferromagnetism and paramagnetism, respectively. At 50 K, the Arrott plot indicates a FM ground state. The isothermal $M(H)$ measurements are therefore consistent with a PM to FM to AF sequence of ordering transitions upon cooling from RT. No magnetic hysteresis is evident from the measurement at 50 K indicating that NdCoAsO is an extremely soft ferromagnet without any sizable remnant magnetization.

The temperature dependence of the electrical resistivity of NdCoAsO is typical of that of a good metal [RRR = 25; Fig. 1(a)]. The magnetic ordering transitions do not result in large

TABLE I. Lattice constants, refined atomic parameters, selected bond distances and angles, and fit statistics for the combined Rietveld fits to synchrotron x-ray and neutron powder-diffraction data for selected $NdFe_{1-x}Co_xAsO$ compositions. Space group $P4/nmm$; Nd on $2c(1/4,1/4,z)$; Fe/Co on $2b(3/4,1/4,1/2)$; As on $2c(1/4,1/4,z)$; O on $2a(1/4,3/4,0)$.

$x_{nominal}$		0.075	0.125	0.175	1.00
	a axis (Å)	3.96754(1)	3.96711(3)	3.96759(4)	3.98724(1)
	c axis (Å)	8.58069(5)	8.5611(1)	8.5462(1)	8.31835(4)
	Volume (Å^3)	135.072(1)	134.734(1)	134.532(1)	132.246(1)
Nd	U_{iso} (Å^2)	0.0041(1)	0.0046(1)	0.0049(1)	0.0060(1)
	z	0.13911(3)	0.13962(4)	0.14004(6)	0.14221(5)
	Occ.	1.00	1.00	1.00	1.00
Fe/Co	U_{iso} (Å^2)	0.0049(1)	0.0050(2)	0.0049(3)	0.0066(2)
	Fe-occ.	0.918(4)	0.886(6)	0.827(8)	0
	Co-occ.	0.076(4)	0.123(6)	0.180(8)	0.996(2)
	Tot-occ.	0.994(5)	1.009(8)	1.007(11)	0.996(2)
As	U_{iso} (Å^2)	0.0057(1)	0.0057(1)	0.0060(2)	0.0059(1)
	z	0.65681(5)	0.65577(8)	0.6549(1)	0.65066(8)
	Occ.	1.011(2)	1.024(3)	1.019(3)	1.003(2)
O	U_{iso} (Å^2)	0.0047(3)	0.0048(4)	0.0029(6)	0.0036(3)
	Occ.	0.978(4)	0.962(6)	0.980(8)	1.000(4)
	$x_{Rietveld}$	0.076(4)	0.122(6)	0.178(8)	0.996(2)
	d(Fe/Co-As) (Å)	2.3970(3)	2.3902(4)	2.3850(5)	2.3546(3)
	∠As-(Fe/Co)-As (deg)	111.70(2)	112.17(3)	112.56(4)	115.70(3)
	∠As-(Fe/Co)-As (deg)	108.37(1)	108.14(1)	107.95(2)	106.45(1)
	χ^2	3.1	3.2	5.2	3.1
NPD	wR_p	3.6	3.6	3.3	3.0
	R_p	2.5	2.5	2.4	2.3
	R_F^2	2.9	2.5	2.8	3.0
XRD	wR_p	7.9	8.7	12.9	10.1
	R_p	5.4	6.2	8.7	6.8
	R_F^2	2.5	2.7	7.8	3.5
	NdAs (wt%)	1.4(1)	6.3(1)	3.4(1)	8.6(1)
	CoAs (wt%)				7.3(3)
	Nd_2O_3 (wt%)	1.1(1)	3.4(1)	2.3(1)	

anomalies in $R(T)$ but are evident in dR/dT, which shows a maximum at ~85 K and a minimum at ~9 K [Fig. 1(a)]. The slope remains positive throughout revealing that the sample is metallic over the entire temperature range.

The magnetic ordering in NdCoAsO was further investigated using high-flux neutron powder diffraction on a 2 g polycrystalline sample. Patterns were collected for 2 h each at 1.7, 15, 40, 70, and 100 K. At 1.7 K, long-range AF order was confirmed by the presence of magnetic Bragg reflections that were not present in the 5 K synchrotron powder-diffraction pattern. These reflections were all indexed on a tetragonal cell doubled along the crystallographic c direction ($a_m=a_N$, $c_m=2c_N$, where the subscript m denotes magnetic and N the nuclear cell). The indexing of the most prominent magnetic reflections is given in Fig. 1(c). Upon heating to 15 K, the AF reflections disappear in agreement with the magnetic susceptibility data. Careful subtraction of the 100 and 15 K data revealed weak magnetic contributions to the nuclear (001) and (002) Bragg reflections. Similar FM intensities were also evident in the 40 K pattern but at 70 K there is no evidence for magnetic Bragg diffraction. This apparent disagreement with susceptibility data is most likely due to the small ordered FM cobalt moment close to T_C. The possible FM and AF magnetic structures were analyzed using

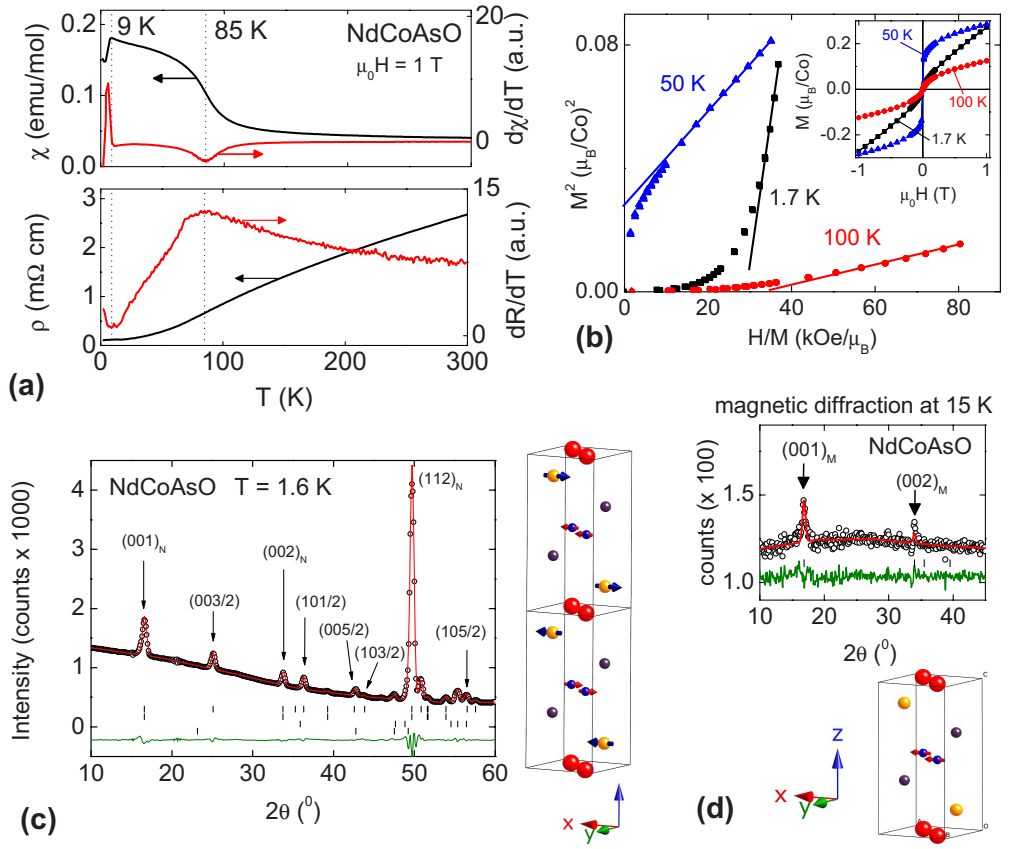

FIG. 1. (Color online) This figure summarizes the measurements on NdCoAsO. Panel (a) shows the temperature dependence of the ZFC magnetic susceptibility (χ) and electrical resistivity (ρ) and their temperature derivatives. Panel (b) shows Arrott plots derived from the isothermal $M(H)$ measurements (shown in the inset). Panel (c) shows the Rietveld fits to the 1.7 K neutron powder-diffraction data (fit statistics: wR_p=3.5%, R_p=2.3%, and R_F^2=8.4%) and a representation of the magnetic structure at that temperature. The tick marks are from top to bottom: magnetic phase, NdCoAsO, CoAs, and NdAs. Panel (d) shows the Rietveld fit to the 15–100 K difference neutron powder-diffraction pattern and a schematic representation of the fitted ferromagnetic magnetic structure.

representational analysis. These calculations were performed using version 2K of the program SARAH representational analysis.[35] In both the FM ($\mathbf{k}$=0) and AF [$\mathbf{k}$=(0 0 1/2)] states all 16 symmetry elements of the $P4/nmm$ space group leave the magnetic propagation vector ($\mathbf{k}$) invariant or transform it into an equivalent vector and thus constitute the small group $G_{\mathbf{k}}$. In the FM state, the decomposition of the magnetic representation Γ_{Mag} in terms of the irreducible representations (IRs) of $G_{\mathbf{k}}$ for the Co site is $1\Gamma_3^1+1\Gamma_6^1+1\Gamma_9^2+1\Gamma_{10}^2$. The representations used are after Kovalev[36] and the character table is given in Table I (supplementary material).[37] The resulting basis vectors for the two independent cobalt atoms are given in Table II. The allowed models correspond to an easy-axis ferromagnet (Γ_3^1), an easy-plane ferromagnet (Γ_9^2), and two checkerboard antiferromagnets with moments along the c direction (Γ_6^1) or in the basal plane (Γ_{10}^2), respectively. The solutions with moments in the basal plane are no longer tetragonal and therefore independent m_x and m_y components are allowed.[38] The absence of a measurable lattice distortion, however, prevents their unique determination. In the AF state the decomposition is $\Gamma_{\mathrm{Mag}}=1\Gamma_2^1+1\Gamma_7^1+1\Gamma_9^2+1\Gamma_{10}^2$ and $\Gamma_{\mathrm{Mag}}=1\Gamma_2^1+1\Gamma_3^1+1\Gamma_9^2+1\Gamma_{10}^2$ for the Co and Nd

TABLE II. Basis vectors $[m_x,m_y,m_z]$ for the space group $P4/nmm$ with $\mathbf{k}$=0 and $\mathbf{k}$=(0 0 1/2). Co1: (1/4, 3/4, 1/2); Co2: (3/4, 1/4, 1/2); Nd1: (1/4, 1/4, 0.14); Nd2: (3/4, 3/4, 0.86); coordinates in crystallographic cell.

	$\mathbf{k}$=0				$\mathbf{k}$=(0 0 1/2)		
	Γ_3^1	Γ_6^1	Γ_9^2	Γ_{10}^2	Γ_2^1	Γ_9^2	Γ_{10}^2
Co1	$[0\ 0\ m_z]$	$[0\ 0\ m_z]$	$[m_x\ m_y\ 0]$	$[m_x\ m_y\ 0]$	$[0\ 0\ m_z]$	$[m_x\ m_y\ 0]$	$[m_x\ m_y\ 0]$
Co2	$[0\ 0\ m_z]$	$[0\ 0\ -m_z]$	$[m_x\ m_y\ 0]$	$[-m_x\ -m_y\ 0]$	$[0\ 0\ m_z]$	$[-m_x\ -m_y\ 0]$	$[m_x\ m_y\ 0]$
Nd1					$[0\ 0\ m_z]$	$[m_x\ m_y\ 0]$	$[m_x\ m_y\ 0]$
Nd2					$[0\ 0\ m_z]$	$[-m_x\ -m_y\ 0]$	$[m_x\ m_y\ 0]$

sites, respectively. In the case of a second-order phase transition, Landau theory states that only a single IR becomes critical. This leaves the Γ_2^1, Γ_9^2, and Γ_{10}^2 symmetries for combined Nd and Co ordering. The unit cell contains two independent Co and two independent Nd sites with basis vectors as given in Table II. The Γ_2^1 and Γ_{10}^2 solutions have FM Co and FM Nd planes (coupled AF) with moments constrained along the c direction and in the basal plane, respectively. The Γ_9^2 solution has AF Co planes and FM Nd planes (coupled AF). The presence of only magnetic (00l) reflections in the FM state reveals that the ordered moment is constrained to the basal plane and that the Γ_9^2 solution is the correct one. Rietveld fitting gives an ordered moment of 0.30(1) μ_B at 15 K and 0.26(1) μ_B at 40 K. A representation of the magnetic structure is shown in Fig. 1(d). Attempts to fit the magnetic intensities to any of the other three models in Table II were not successful. Subtraction of the 15 and 1.7 K data showed that the FM contribution to the (00l) reflections has disappeared at base temperature. Trial Rietveld refinements quickly established that the Γ_2^1 and Γ_9^2 models do not give good fits to the observed magnetic intensities. The Γ_{10}^2 solution in contrast yields an excellent fit to the data. In this model, adjacent FM Nd layers couple AF, and the FM Co layer at $z=1/4$ couples AF with the FM Co layer at $z=3/4$, and adjacent Co and Nd moments are antiparallel. All moments are constrained to the basal plane and Rietveld fitting gives $m_{Co}=0.26(6)$ μ_B and $m_{Nd}=1.39(4)$ μ_B at 1.7 K. The final Rietveld fit and a schematic representation of the magnetic structure are given in Fig. 1(c).

IV. STRUCTURE AND PROPERTIES OF $NdFe_{1-x}Co_xAsO$ $(0<x<1)$

Inspection of the synchrotron x-ray powder-diffraction patterns revealed that all prepared samples have the tetragonal $P4/nmm$ structure at RT. The lattice constants were obtained from Rietveld fits and revealed that the crystallographic c/a ratio varies linearly with x over the entire composition range $(0\leq x\leq 1)$ as shown in Fig. 2. The solid circles are selected samples where the composition has been confirmed from combined Rietveld fits to synchrotron x-ray and neutron powder-diffraction data. The linear dependence suggests that the c/a ratio can be used as an experimental measure of the composition. For most compositions, the agreement between the nominal and calculated (c/a-derived) compositions is within 1–3 esd's (Table III). For some samples (e.g., $x_{nominal}=0.10$) a larger deviation is found, which signals the formation of impurities that change the stoichiometry of the main phase. Use of the calculated compositions results in a smoother x dependence of the refined lattice constants, bond lengths, and bond angles. In addition, it discriminates between samples with the same nominal composition but different SC transition temperatures and vice versa (Table III). For these reasons, the compositions (x) used in this paper are the ones calculated from the c/a ratio unless stated otherwise. The x dependences of the lattice constants are shown in Fig. 2. The a axis is almost constant at low doping levels, in agreement with other cobalt-doped superconductors,[17,39] and increases moderately for $x>0.25$.

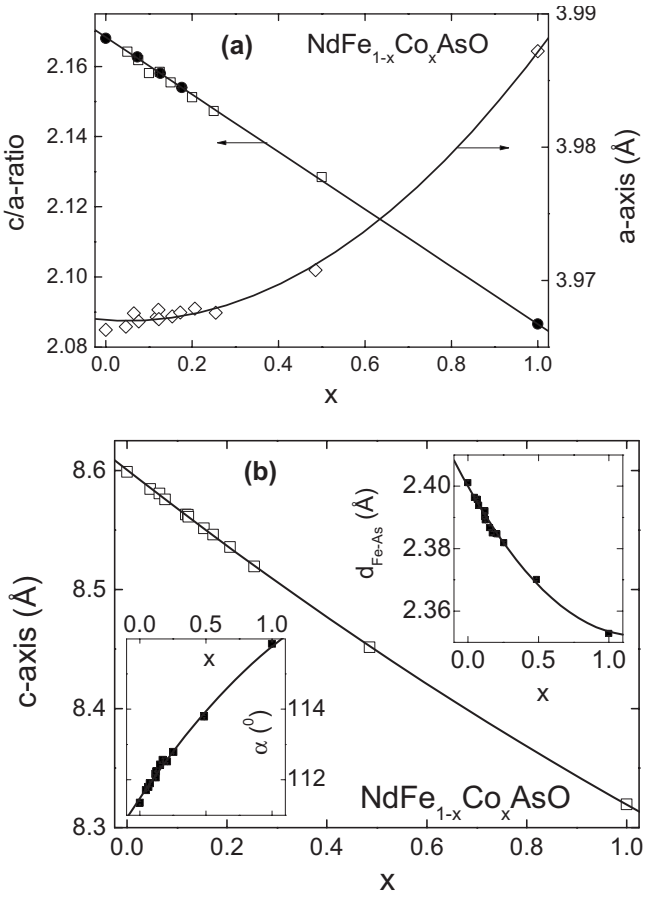

FIG. 2. (a) Left axis: crystallographic c/a ratio versus $x_{nominal}$ for $NdFe_{1-x}Co_xAsO$. The fitted line is $c/a=-0.0814(5)x+2.167\ 99(4)$. Right axis: the a axis versus the composition derived from the c/a ratio (x). (b) Crystallographic c axis plotted versus x. The insets show the x dependence of the Fe-As bond distance and the tetrahedral As-Fe-As angle (α, defined in the inset of Fig. 9) for the $NdFe_{1-x}Co_xAsO$ series. The solid lines are guides for the eyes.

In contrast, the c axis contracts rapidly. The (Fe/Co)-As bond lengths show a gradual contraction from 2.40 Å for $x=0$ to 2.35 Å for $x=1$, while the tetrahedral angle increases from 111.4° ($x=0$) to 115.7° [$x=1$; inset of Fig. 2(b)].

In order to independently confirm the composition of selected samples, a combined Rietveld analysis of room-temperature synchrotron x-ray and neutron powder-diffraction data was undertaken. This allows the simultaneous refinement of the total transition-metal site occupancy and the iron to cobalt ratio. The total occupancy is effectively obtained from fitting the x-ray data as there is no significant scattering contrast between Fe and Co, while the difference in neutron scattering length [Fe: 9.45 fm, Co: 2.49 fm] allows for the determination of the Co/Fe ratio. Four compositions were studied: $x_{nominal}=0.075$, 0.125, 0.175, and 1, while the $x=0$ composition has been previously reported.[29] In these refinements, the lattice constants were kept at the synchrotron x-ray values and the neutron wavelength [$\lambda=1.3010(2)$ Å] was refined to fit the neutron-diffraction data. The fit to the $x_{nominal}=0.125$ x-ray and neutron powder-diffraction data is shown in Fig. 3. The other fits are given in Fig. 1 (supplementary material). The results of

TABLE III. Crystallographic c/a ratios, compositions from the c/a ratio (x), compositions from Rietveld fits (x_{Rietveld}), and critical temperatures from the onset of diamagnetism and resistive transition midpoint for the $NdFe_{1-x}Co_xAsO$ series.

x_{nominal}	c/a	x [a]	x_{Rietveld}	T_c, χ_{onset} (K)	T_c, R_{mid} (K)
0	2.16799(4)	0			
0.05	2.16420(4)	0.047(2)		<1.8	<1.8
0.075 (NPD)	2.16272(4)	0.065(2)	0.076(4)	12.8(2)	9.2(2)
0.075	2.16180(4)	0.076(2)		15.0(2)	
0.10	2.15808(4)	0.122(2)		16.7(2)	16.2(2)
0.125	2.15840(4)	0.118(2)		16.5(2)	16.0(2)
0.125 (NPD)	2.15802(4)	0.123(2)	0.122(6)	16.6(2)	
0.15	2.15546(4)	0.154(2)		15.1(2)	
0.175 (NPD)	2.15398(4)	0.172(2)	0.178(8)	13.4(2)	12.6(2)
0.2	2.15121(4)	0.206(2)		<1.8	<1.8
0.25	2.14726(4)	0.255(2)		<1.8	<1.8
0.50	2.12845(4)	0.486(2)			
1	2.08657(4)	1	0.996(2)		

[a] $c/a=-0.0814(5)x+2.167\ 99(4)$.

the combined Rietveld fits are summarized in Table I. They reveal that the total occupancy of the transition-metal site is unity in all cases and that the refined Fe and Co fractions are within a single estimated standard deviation of the nominal values. This result is robust as trials with randomly picked Fe and Co fractions always recovered the result shown in Table I. The refinement of the other site occupancies indicates slightly larger than full occupancies on the As site and slightly reduced O-site occupancies (Table I). It is not clear if these are significant but we note that in a simple ionic model with As^{3-} and O^{2-} the charge doping effects cancel out. In addition, oxygen deficient 1111-type samples, such as $NdFeAsO_{1-d}$, have only been prepared using high-pressure high-temperature synthesis routes suggesting that ambient pressure routes do not normally lead to oxygen deficiencies.[40]

Variable temperature synchrotron x-ray diffraction was used to follow the $P4/nmm$ (T) to $Cmma$ (O) transition associated with the AF ordering that occurs in 1111-type parent materials. In case of NdFeAsO ($x=0$), a broad transition with initial broadening of Bragg reflections at ~160 K followed by a full splitting at ~140 K has been reported.[20,41] The latter temperature corresponds to the onset of long-range AF order of the Fe spins.[42] For $NdFe_{1-x}Co_xAsO$ [$x=0.047(2)$, $x=0.065(2)$, and $x=0.123(2)$], data were collected on heating from 4 K. At low temperatures a broadening of reflections with Miller indexes $h\neq 0$ and $k\neq 0$, consistent with the well established $T\rightarrow O$ transition, was evident (Fig. 2; supplementary material). However, no peak splitting occurs down to the lowest measured temperatures. Structural refinements using the orthorhombic $Cmma$ model showed a clear divergence of the a and b axes for $x=0.047(2)$ and $x=0.065(2)$, respectively. In contrast, refinements for $x=0.122(2)$ showed no evidence for a structural distortion as Rietveld fits with the $P4/nmm$ and $Cmma$ structural models gave the same residuals and almost identical a and b axes. The slight broadening evident for $x=0.122(2)$ in Fig. 2 (supplementary material) can therefore not be attributed to the $T\rightarrow O$ transition. The temperature dependence of the lattice constants is shown in Fig. 4, where the orthorhombic cell constants (a_O,b_O) have been divided by $\sqrt{2}$. The lattice constants above the $T\rightarrow O$ transition were obtained from fits to the $P4/nmm$ structural model. The transition temperatures were taken from the onset temperature of orthorhombic strain, $s=(a_O-b_O)/(a_O+b_O)$, and are 72(2) K [$x=0.047(2)$] and 64(2) K [$x=0.065(2)$], respectively (Fig. 4). The low field ZFC susceptibilities for the $NdFe_{1-x}Co_xAsO$ solid solution series are given in Fig. 5. Superconducting transitions are observed for samples with $0.065(2)\leq x\leq 0.172(2)$. The transition temperatures were taken from the diamagnetic onset temperature and are summarized in Table III. This reveals almost identical values of 16.5(2) K for optimally doped samples near $x=0.12$ [$x=0.118(2)$, $x=0.122(2)$, and $x=0.123(2)$]. The diamagnetic shielding fractions vary from 30%–70% of $4\pi\chi$ for samples with $x=0.12$ and are lower on the underdoped and overdoped sides as are the critical temperatures. The SC transitions were confirmed by electrical resistance measurements. The normalized resistances $R/R_{300\ \mathrm{K}}$ are given in Fig. 6. The 300 K resistivities fall between 5 mΩ cm for $x=0$ and 2 mΩ cm for $x=1$. The normal state resistance for $x=0$ shows the familiar drop below $T\sim 160$ K with the maximum slope dR/dT at 140 K. These temperatures correspond to the onset of the $T\rightarrow O$ transition and AF order, respectively.[20] Samples with $x>0.2$ have metallic temperature dependences indicating a transition to more conventional metallic behavior on the overdoped side. On the underdoped side, increasing x suppresses the SDW transition and no large anomaly in $R(T)$ is evident for any of the SC samples. At low temperatures SC transitions are evident. The transition temperatures were taken from the 50% of normal state resistance values ($0.5R_N$) and are listed in Table III. The obtained values are in good agreement with the values from the magnetic susceptibility measurements. The widths of the resistive transitions were determined by taking the difference

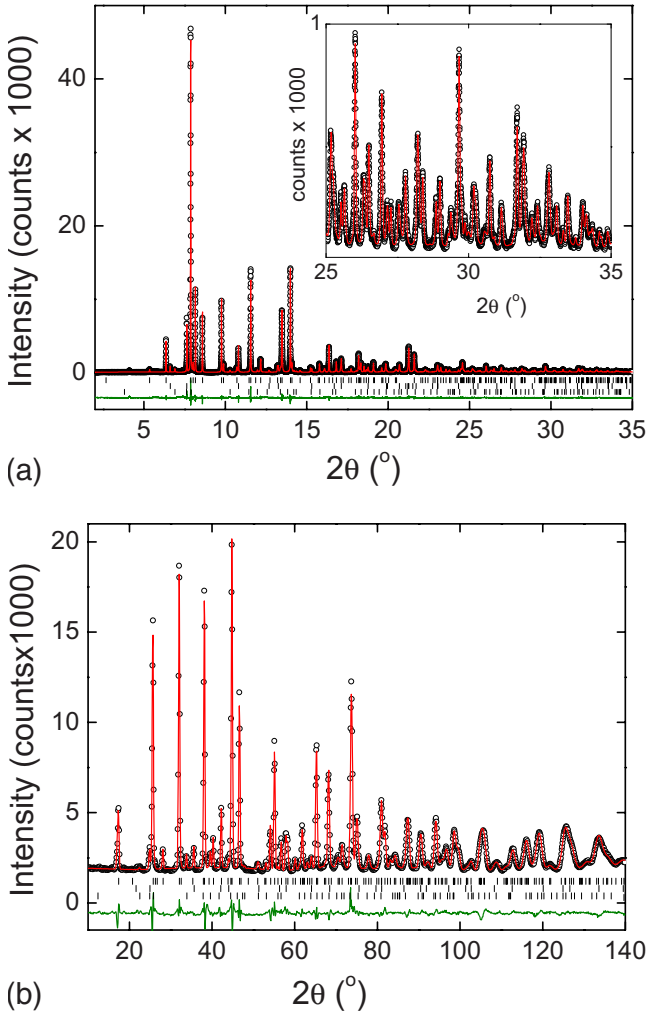

FIG. 3. (Color online) Combined Rietveld fit to room-temperature synchrotron x-ray (a) and neutron powder-diffraction data (b) for a sample with $x_{nominal}=0.125$. Observed data are indicated by open circles, the fit by the (solid) red line, and the difference curve (solid green line) is shown at the bottom. Bragg positions are indicated by vertical markers. The bottom markers correspond to NdAs and Nd_2O_3 impurities (Table I).

between $0.9R_N$ and $0.1R_N$ and are ~2 K wide for the optimally doped samples ($x=0.12$), ~5 K for $x=0.065(2)$, and ~3 K for $x=0.0172(2)$. This is comparable to other polycrystalline 1111-type cobalt-doped superconductors including $LaFe_{1-x}Co_xAsO$ (Refs. 13 and 17) and $SmFe_{1-x}Co_xAsO$ (Ref. 17), and polycrystalline samples of $Ba(Fe_{1-x}Co_x)_2As_2$.[9] The field dependence of $R(T)$ in the vicinity of the SC transition was studied up to 9 T for samples with $x=0.065(2)$, $x=0.118(2)$, and $x=0.172(2)$. The results are shown in the left panels of Fig. 7 and reveal a significant suppression of T_c with applied magnetic field. The upper critical fields were determined at the temperatures of the 10%, 50%, and 90% reduction in the normal state resistance. The results are plotted in the right-hand side panels of Fig. 7. In all samples, an initial rapid reduction in small applied fields $\mu_0 H < 0.5$ T is evident. This is followed by an approximately linear decrease for $\mu_0 H > 1$ T, which shows no sign of saturation. The slopes are dependent on the used resistance criterion signaling a broadening of the transition in applied magnetic fields. This is characteristic for type-II superconductors and was also observed in the $LaFe_{1-x}Co_xAsO$ series.[13] Using the $0.5R_N$ criterion, almost identical slopes of −2.5(1) T K^{-1} [$x=0.065(2)$], −2.3(1) T K^{-1} [$x=0.118(2)$], and −2.3(1) T K^{-1} [$x=0.172(2)$] were obtained from linear fits between $1 \le \mu_0 H \le 9$ T. The linear dependence of $H_{c2}(T)$ near T_c suggests that the Werthamer-Helfand-

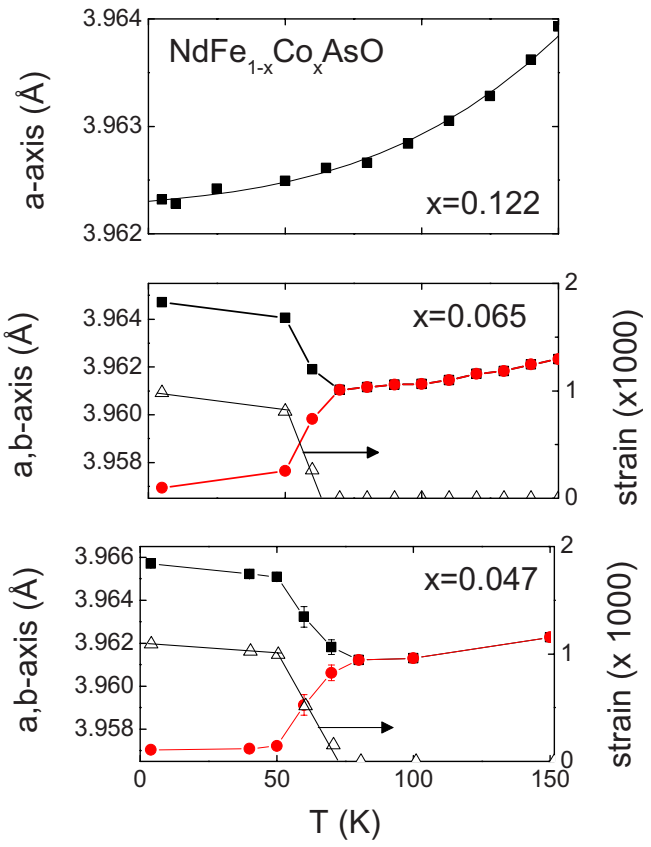

FIG. 4. (Color online) Temperature dependence of the crystallographic basal plane lattice constants and orthorhombic strain for selected low-x $NdFe_{1-x}Co_xAsO$ compositions.

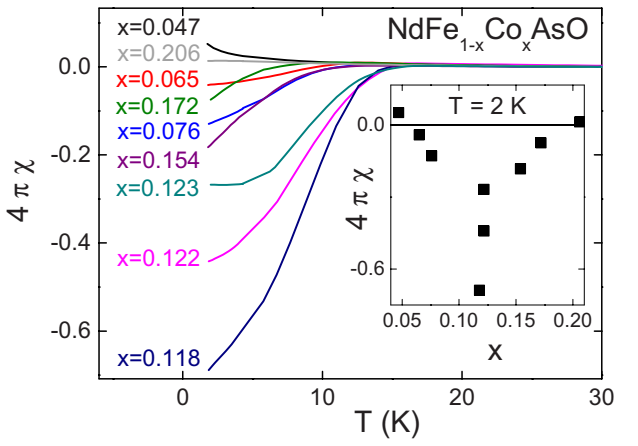

FIG. 5. (Color online) Temperature dependence of the low field magnetic susceptibilities for $NdFe_{1-x}Co_xAsO$. The inset shows x dependence of the diamagnetic fraction at 2 K.

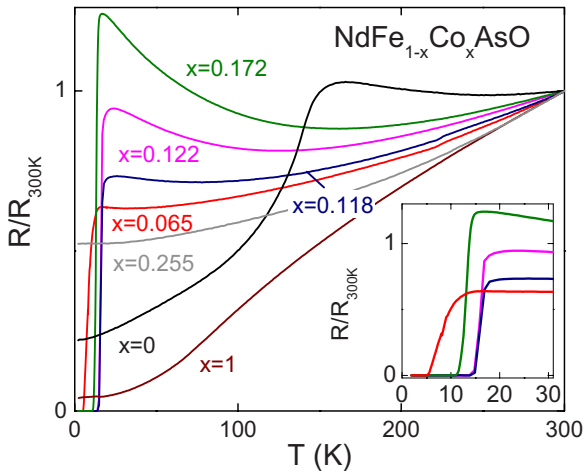

FIG. 6. (Color online) Temperature dependence of the normalized electrical resistance ($R/R_{300\ \mathrm{K}}$) for $NdFe_{1-x}Co_xAsO$. The inset illustrates the superconducting transitions.

Hohenberg model, which predicts $H_{c2}(0)=0.69\ T_c[dH_{c2}/dT]$, can be used to estimate the upper critical field at zero temperature.[43] This yields the following estimates: $H_{c2}(0)=14(1)$ T for $x=0.065(2)$, $H_{c2}(0)=26(1)$ T for $x=0.118(2)$, and $H_{c2}(0)=21(1)$ T for $x=0.172(2)$. The SC coherence length (ξ) is given by $\xi^2(0)=\Phi_0/2\pi H_{c2}(0)$, where $\Phi_0=2.07\times10^{-7}$ Oe cm^2, yielding a coherence length of 36(1) Å for $x=0.118(2)$.

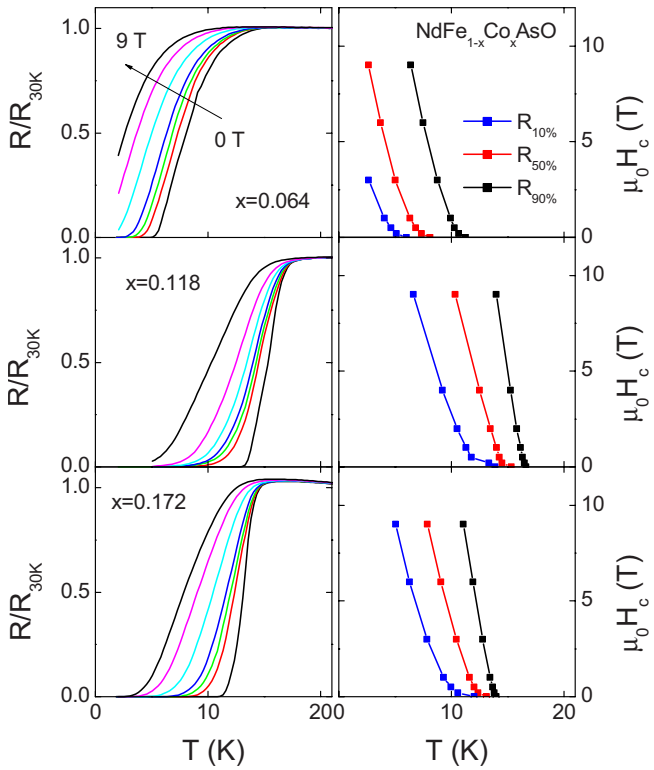

FIG. 7. (Color online) Temperature and field dependences of the electrical resistance for selected $NdFe_{1-x}Co_xAsO$ compositions. $H_{c2}(T)$ derived from 10% ($0.1R_N$), 50% ($0.5R_N$), and 90% ($0.9R_N$) resistance drops are shown on the right-hand side.

V. DISCUSSION

Like the isostructural *R*FeAsO high-T_c parent materials NdCoAsO exhibits significant interplay between the rare-earth and transition-metal sublattices. Below 85 K, NdCoAsO is an itinerant FM with a small ordered cobalt moment of 0.3 μ_B constrained to the *ab* plane. This is analogous to LaCoAsO, which has a Curie temperature of ~60 K and a moment of 0.5 μ_B,[13,22] and consistent with calculations for LaCoAsO that reveal a spin-polarized band structure with a small ordered moment.[22] Our Arrott plots suggest a linear dependence of M^2 on H/M in large fields typical of weak itinerant ferromagnets such as $ZrZn_2$ but different to the "anomalous" M^4 dependence reported for LaCoAsO.[23] More extensive measurements are needed to investigate this. Below 9 K, Nd spin ordering transforms NdCoAsO to an AF metal. Both the FM and AF transitions are evident in the temperature derivative of the resistance but do not result in large anomalies as observed for *R*FeAsO. In the *R*FeAsO materials the Fe spins order in a striped pattern with a small ordered moment of ~0.4 μ_B for all *R* from spectroscopic methods such as Mossbauer and μSR.[25] Neutron powder diffraction, in contrast, suggests a wider spread of 0.3–0.8 μ_B,[26] which Maeter *et al.* have attributed to an induced magnetization on the *R* sublattice below T_{SDW} that contributes to the "Fe" magnetic Bragg reflections.[25] It is not clear from our measurements whether this is important but the almost constant Co moment between 1.7 and 40 K (~0.3 μ_B) suggests that there is no significant induced "Nd contribution." The spectroscopic measurements also suggest that the *R* spin ordering does not have any effect on the magnitude of the Fe moment, while for neutron powder diffraction increases have been reported, in particular, for *R*=Nd.[42,44] In the current case, the available evidence points toward an unchanged Co moment. However, we note that in symmetry unrestricted refinements (i.e., by allowing canting out of the basal plane) it is possible to obtain solutions with $m_{Co}=0.9(2)$ μ_B but these are characterized by large correlations and large estimated standard deviations. Trial refinements with noncollinear *R* ordering analogous to that reported for CeFeAsO (Ref. 8) did not give satisfactory fits to the data. The fitted Nd moment is 1.39(4) μ_B, which is comparable to the value for NdFeAsO [1.55(4) μ_B].[29,44]

The lattice constants, bond distances, and angles for $NdFe_{1-x}Co_xAsO$ change gradually, signaling the formation of a solid solution, as confirmed by Rietveld refinement of the Fe/Co occupancies of selected samples against neutron and synchrotron x-ray data. Furthermore, the structural analysis reveals that the c/a ratio can be used as an experimental measure of the composition [Fig. 2(a)]. This is valid because the combined x-ray and neutron refinements presented in Table I confirm that the only significant compositional change throughout the series is the Fe/Co ratio. The twofold As-Fe-As tetrahedral angle (α, defined in Fig. 9) increases with x. This is in contrast to most other forms of chemical doping and may in part explain why cobalt doping has not yielded the high T_c's observed in other electron-doped superconductors, such as $NdFeAsO_{1-x}F_x$ and $NdFeAsO_{1-d}$, despite having the same nominal amount of doping. The chemical disorder introduced by mixing Fe/Co on the same crystallo-

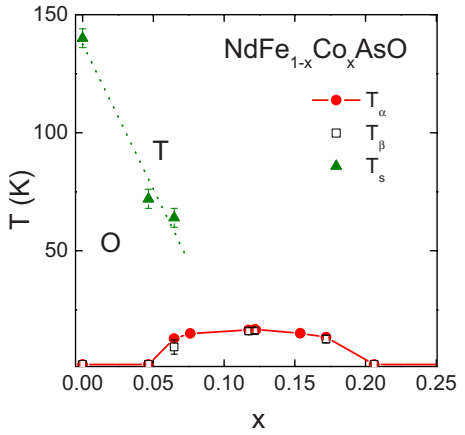

FIG. 8. (Color online) Temperature-composition phase diagram for $NdFe_{1-x}Co_xAsO$ showing the suppression of the structural $T \rightarrow O$ phase transition with increasing Co concentration and the superconducting dome. The data points for the $T \rightarrow O$ structural transition (T_s) were obtained from synchrotron x-ray powder diffraction, while the superconducting T_c values were obtained from the diamagnetic onset temperatures (T_α; red circles) and midpoint resistances (T_β; black squares). Error bars indicate 10% and 90% of the resistive transition. The green dotted line is a linear fit to the T_s data.

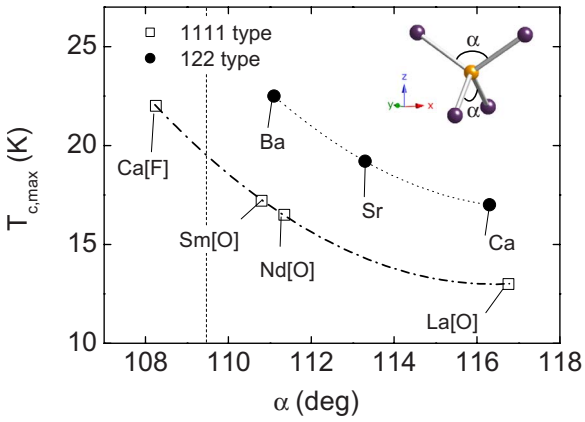

FIG. 9. (Color online) Variation in the superconducting T_c with tetrahedral As-Fe-As angle (defined in the inset) for well-characterized 122-type $AE(Fe_{1-x}Co_x)_2As_2$ (solid circles) and 1111-type $RFe_{1-x}Co_xAsO$ and $AEFe_{1-x}Co_xAsF$ (open squares) superconductors. The line is intended as a guide for the eyes. Data were taken from the following references: Ca[F] (Ref. 18), La[O] (Refs. 13 and 17), Sm[O] (Ref. 17), Ca (Ref. 15), Sr (Ref. 16), and Ba (Ref. 39).

graphic site is also expected to have a detrimental effect on the maximum attainable T_c's. The variable temperature synchrotron diffraction study reveals subtle structural distortions consistent with the well established $T \rightarrow O$ structural transition upon cooling for samples with $x=0.046(2)$ and $x=0.065(2)$. This confirms that replacement of Fe with Co suppresses the $T \rightarrow O$ transition and the associated SDW.

The phase diagram for low cobalt substitutions is presented in Fig. 8 and reveals the presence of a SC dome with limiting compositions $0.05 < x < 0.20$. The maximum critical temperature is 16.5(2) K for $x=0.12$. The underdoped samples ($x \leq 0.075$) have the orthorhombic *Cmma* structure. The presence of a "dome" and possible overlap between magnetic and SC regions is consistent with results published for other 1111- and 122-type cobalt-doped superconductors although the existence of phase coexistence is still under debate.[9,17,18,45] The critical field, $H_{c2}(T)$, increases by approximately 2.3(1) T K^{-1} for the three measured compositions upon cooling below T_c. This is smaller than for "indirect" (not Fe-site) electron-doped superconductors, such as $NdFeAsO_{1-x}F_x$, where values of 4–5 T K^{-1} have been observed.[46] However, similar values are reported for other cobalt-doped superconductors[13,39] suggesting that the superconductivity in these materials is less robust against applied magnetic fields.

Finally, the maximum observed critical temperatures ($T_{c,\max}$) for well-characterized cobalt-doped superconductors are plotted in Fig. 9 against the tetrahedral As-Fe-As angle (α). The angles used are for the parent materials as α is not commonly reported for doped compositions. However, this does not affect the reported trends significantly as the increase in α upon cobalt doping is expected to be similar in all materials. The following observations can be made: (1) $T_{c,\max}$ increases as α tends toward the cubic value. This is in agreement with the literature for indirectly doped superconductors,[8,19,47] although there is no evidence for a maximum occurring at the ideal tetrahedral angle. (2) The 122-type materials have higher T_c's than the 1111-type for a given value of α. This contrasts the situation for indirect doping where the largest T_c's up to 55 K are obtained for electron-doped 1111 phases such as $NdFeAsO_{1-x}F_x$, while the hole-doped 122 phases with a smaller separation between Fe_2As_2 planes are limited to 38 K for $Ba_{1-x}K_xFe_2As_2$ (both parents have $\alpha \sim 111.2°$). This suggests that were it possible to electron dope the 122 superconductors via chemical substitutions on the *AE* site higher T_c's than 55 K may be achieved.

To summarize, we have investigated the structures and properties of the $NdFe_{1-x}Co_xAsO$ series ($0 \leq x \leq 1$). For low cobalt doping, the phase diagram contains a superconducting dome ($0.05 < x < 0.20$, maximum $T_c = 16.5(2)$ K for $x=0.12$). Samples with $x \leq 0.075$ have the orthorhombic *Cmma* structure at low temperatures. NdCoAsO is an itinerant ferromagnet ($T_C = 85$ K) with a small cobalt moment (0.3 μ_B) that shows a transition to an antiferromagnetic state at $T_N = 9$ K.

Noted added in proof. Recently, we became aware of a preprint article on NdCoAsO by McGuire *et al.*[48] that supports the results presented here.

ACKNOWLEDGMENTS

J.W.G.B. acknowledges the Royal Society of Edinburgh for financial support and the EPSRC-GB for the provision of beam time at the ILL and ESRF.

[1] Y. Kamihara, T. Watanabe, M. Hirano, and H. Hosono, J. Am. Chem. Soc. **130**, 3296 (2008).

[2] K. Ishida, Y. Nakai, and H. Hosono, J. Phys. Soc. Jpn. **78**, 062001 (2009).

[3] M. V. Sadovskii, Phys. Usp. **51**, 1201 (2008).

[4] D. J. Singh and M. H. Du, Phys. Rev. Lett. **100**, 237003 (2008).

[5] I. I. Mazin, D. J. Singh, M. D. Johannes, and M. H. Du, Phys. Rev. Lett. **101**, 057003 (2008).

[6] C. W. Chu and B. Lorenz, Physica C **469**, 385 (2009).

[7] A. J. Drew, C. Niedermayer, P. J. Baker, F. L. Pratt, S. J. Blundell, T. Lancaster, R. H. Liu, G. Wu, X. H. Chen, I. Watanabe, V. K. Malik, A. Dubroka, M. Rossle, K. W. Kim, C. Baines, and C. Bernhard, Nature Mater. **8**, 310 (2009).

[8] J. Zhao, Q. Huang, C. de la Cruz, S. L. Li, J. W. Lynn, Y. Chen, M. A. Green, G. F. Chen, G. Li, Z. Li, J. L. Luo, N. L. Wang, and P. C. Dai, Nature Mater. **7**, 953 (2008).

[9] J. H. Chu, J. G. Analytis, C. Kucharczyk, and I. R. Fisher, Phys. Rev. B **79**, 014506 (2009).

[10] X. F. Wang, T. Wu, G. Wu, R. H. Liu, H. Chen, Y. L. Xie, and X. H. Chen, New J. Phys. **11**, 045003 (2009).

[11] H. Chen, Y. Ren, Y. Qiu, W. Bao, R. H. Liu, G. Wu, T. Wu, Y. L. Xie, X. F. Wang, Q. Huang, and X. H. Chen, Europhys. Lett. **85**, 17006 (2009).

[12] H. Luetkens, H. H. Klauss, M. Kraken, F. J. Litterst, T. Dellmann, R. Klingeler, C. Hess, R. Khasanov, A. Amato, C. Baines, M. Kosmala, O. J. Schumann, M. Braden, J. Hamann-Borrero, N. Leps, A. Kondrat, G. Behr, J. Werner, and B. Buchner, Nature Mater. **8**, 305 (2009).

[13] A. S. Sefat, A. Huq, M. A. McGuire, R. Y. Jin, B. C. Sales, D. Mandrus, L. M. D. Cranswick, P. W. Stephens, and K. H. Stone, Phys. Rev. B **78**, 104505 (2008).

[14] A. S. Sefat, R. Y. Jin, M. A. McGuire, B. C. Sales, D. J. Singh, and D. Mandrus, Phys. Rev. Lett. **101**, 117004 (2008).

[15] N. Kumar, R. Nagalakshmi, R. Kulkarni, P. L. Paulose, A. K. Nigam, S. K. Dhar, and A. Thamizhavel, Phys. Rev. B **79**, 012504 (2009).

[16] A. Leithe-Jasper, W. Schnelle, C. Geibel, and H. Rosner, Phys. Rev. Lett. **101**, 207004 (2008).

[17] C. Wang, Y. K. Li, Z. W. Zhu, S. Jiang, X. Lin, Y. K. Luo, S. Chi, L. J. Li, Z. Ren, M. He, H. Chen, Y. T. Wang, Q. Tao, G. H. Cao, and Z. A. Xu, Phys. Rev. B **79**, 054521 (2009).

[18] S. Matsuishi, Y. Inoue, T. Nomura, H. Yanagi, M. Hirano, and H. Hosono, J. Am. Chem. Soc. **130**, 14428 (2008).

[19] C. H. Lee, A. Iyo, H. Eisaki, H. Kito, M. T. Fernandez-Diaz, T. Ito, K. Kihou, H. Matsuhata, M. Braden, and K. Yamada, J. Phys. Soc. Jpn. **77**, 083704 (2008).

[20] P. Jeglic, J. W. G. Bos, A. Zorko, M. Brunelli, K. Koch, H. Rosner, S. Margadonna, and D. Arcon, Phys. Rev. B **79**, 094515 (2009).

[21] M. Rotter, M. Pangerl, M. Tegel, and D. Johrendt, Angew. Chem., Int. Ed. **47**, 7949 (2008).

[22] H. Yanagi, R. Kawamura, T. Kamiya, Y. Kamihara, M. Hirano, T. Nakamura, H. Osawa, and H. Hosono, Phys. Rev. B **77**, 224431 (2008).

[23] H. Ohta and K. Yoshimura, Phys. Rev. B **79**, 184407 (2009).

[24] A. S. Sefat, D. J. Singh, R. Jin, M. A. McGuire, B. C. Sales, and D. Mandrus, Phys. Rev. B **79**, 024512 (2009).

[25] H. Maeter, H. Luetkens, Y. G. Pashkevich, A. Kwadrin, R. Khasanov, A. Amato, A. A. Gusev, K. V. Lamonova, D. A. Chervinskii, R. Klingeler, C. Hess, G. Behr, B. Buchner, and H. H. Klauss, Phys. Rev. B **80**, 094524 (2009).

[26] J. W. Lynn and P. C. Dai, Physica C **469**, 469 (2009).

[27] M. Le Tacon, M. Krisch, A. Bosak, J. W. G. Bos, and S. Margadonna, Phys. Rev. B **78**, 140505 (2008).

[28] K. Kasperkiewicz, J. W. G. Bos, A. N. Fitch, K. Prassides, and S. Margadonna, Chem. Commun. **2009**, 707.

[29] A. Marcinkova, E. Suard, A. N. Fitch, S. Margadonna, and J. W. G. Bos, Chem. Mater. **21**, 2967 (2009).

[30] T. C. Hansen, P. F. Henry, H. E. Fischer, J. Torregrossa, and P. Convert, Meas. Sci. Technol. **19**, 034001 (2008).

[31] A. C. Larson and R. B. Von Dreele, Los Alamos National Laboratory LAUR Report No. 86, 2000 (unpublished).

[32] P. W. Stephens, J. Appl. Crystallogr. **32**, 281 (1999).

[33] P. Quebe, L. J. Terbuchte, and W. Jeitschko, J. Alloys Compd. **302**, 70 (2000).

[34] A. Arrott, Phys. Rev. **108**, 1394 (1957).

[35] A. S. Wills, Physica B **276-278**, 680 (2000).

[36] O. V. Kovalev, *Representations of the Crystallographic Space Groups* (Gordon and Breach Science Publishers, Switzerland, 1993).

[37] See supplementary material at http://link.aps.org/supplemental/10.1103/PhysRevB.81.064511 for the Character Table of the small group Gk, room temperature synchrotron x-ray and neutron diffraction Rietveld profiles for $x=0.075$, $x=0.175$, and $x=100$, and tetragonal to orthorhombic peak broadening observed in synchrotron x-ray powder diffraction for underdoped $NdFe_{1-x}Co_xAsO$ samples.

[38] A. Authier, *International Tables for Crystallography, Volume D* (Kluwer Academic Publishers, Dordrecht, 2003).

[39] N. Ni, M. E. Tillman, J. Q. Yan, A. Kracher, S. T. Hannahs, S. L. Bud'ko, and P. C. Canfield, Phys. Rev. B **78**, 214515 (2008).

[40] K. Miyazawa, K. Kihou, P. M. Shirage, C. H. Lee, H. Kito, H. Eisaki, and A. Iyo, J. Phys. Soc. Jpn. **78**, 034712 (2009).

[41] M. Fratini, R. Caivano, A. Puri, A. Ricci, Z. A. Ren, X. L. Dong, J. Yang, W. Lu, Z. X. Zhao, L. Barba, G. Arrighetti, M. Polentarutti, and A. Bianconi, Supercond. Sci. Technol. **21**, 092002 (2008).

[42] Y. Chen, J. W. Lynn, J. Li, G. Li, G. F. Chen, J. L. Luo, N. L. Wang, P. C. Dai, C. de la Cruz, and H. A. Mook, Phys. Rev. B **78**, 064515 (2008).

[43] N. R. Werthamer, E. Helfand, and P. C. Hohenberg, Phys. Rev. **147**, 295 (1966).

[44] Y. Qiu, W. Bao, Q. Huang, T. Yildirim, J. M. Simmons, M. A. Green, J. W. Lynn, Y. C. Gasparovic, J. Li, T. Wu, G. Wu, and X. H. Chen, Phys. Rev. Lett. **101**, 257002 (2008).

[45] C. Lester, J. H. Chu, J. G. Analytis, S. C. Capelli, A. S. Erickson, C. L. Condron, M. F. Toney, I. R. Fisher, and S. M. Hayden, Phys. Rev. B **79**, 144523 (2009).

[46] J. Jaroszynski, F. Hunte, L. Balicas, Y. J. Jo, I. Raicevic, A. Gurevich, D. C. Larbalestier, F. F. Balakirev, L. Fang, P. Cheng, Y. Jia, and H. H. Wen, Phys. Rev. B **78**, 174523 (2008).

[47] J. A. Rodgers, G. B. S. Penny, A. Marcinkova, J.-W. G. Bos, D. A. Sokolov, A. Kusmartseva, A. D. Huxley, and J. P. Attfield, Phys. Rev. B **80**, 052508 (2009).

[48] M. A. McGuire *et al.*, arXiv:0912.4237, Phys. Rev. B (to be published).